Gradient-based Iterative Identification Method for Non-uniformly Sampled Input-nonlinear Systems

Xiyuan Zou, Li Xie, Ruilin Bai, Huizhong Yang

School of Internet of Things Engineering, Jiangnan University, Wuxi,PR China, (e-mail: ws zxy@outlook.com, xieli@jiangnan.edu.cn, bairuilin@hotmail.com, yhz@jiangnan.edu.cn).

Abstract: This paper proposes an identification method of an input-nonlinear system with saturation and dead-zone nonlinearity using the asynchronous input-output data spaced by non-uniform intervals. The piecewise expression of the nonlinear part is simplified as an analytic function with an available switching function. By extending the traditional continuous linear time-invariant processes to non-uniformly sampled input-nonlinear systems, a concise input-output representation model is derived. Based on the key term separation principle and the auxiliary model identification idea, a gradient-based iterative identification algorithm is developed for simultaneously estimating all parameters of the derived model. Through a numerical example, the proposed algorithm shows its superior estimation accuracy compared to the auxiliary model-based forgetting factor stochastic gradient algorithm. Finally, the application to a mathematical model of a two-tank system indicates the effectiveness of the proposed method.

Keywords: input-nonlinear system; Hammerstein system; iterative identification; non-uniform sampling; parameter estimation.

1. INTRODUCTION

Due to nonlinear devices and complex mechanisms, non-linearities are commonly encountered in practical processes such as control systems (Ioanas et al., 2013; Amer et al., 2021), satellite dynamics and chemical and biological processes. Nonlinear systems can be described by block-oriented nonlinear models, including Hammerstein models, Wiener models, Wiener-Hammerstein models and Hammerstein-Wiener models (Schoukens and Tiels, 2017). Hammerstein models refer to the systems composed of a static nonlinear part followed by a linear time-invariant part, which have been employed to describe a class of nonlinear systems with nonlinear input, such as quantization (Xing et al., 2015), hysteresis (Gao et al., 2015), and backlash (Giri et al., 2011). The saturation and dead-zone characteristic is a typical input nonlinearity in engineering practice and widely exists in actuators (Hu et al., 2008), for example, in piezoelectric translators, elec- tric servo motors (Tahoun, 2017), and surface ships (Xia et al., 2013). The existence of the nonlinearity can worsen system performance and even threaten system instability, which tends to bring about severe damage in industry application. Consequently, the research on its analysis, stability and controlling has received extensive attention (Oh and Park, 2000; Dong, 2015). The identification of saturation and dead-zone is of significant interest for further research on it.

Parameter estimation of Hammerstein systems is essential for in-depth analysis and study of linear systems (Pan et al., 2018) and nonlinear systems (Avila et al., 2017). There have been many identification methods proposed for Hammerstein systems with single rate (Pu et al., 2021; Zhang et al., 2017). Liu and Bai presented three iterative algorithms to estimate Hammerstein systems with three kinds of nonlinear blocks, infinite impulse response, the saturation and preload (Liu and Bai, 2007). To handle Hammerstein systems with colored noise, a stochastic algorithm was proposed by combining the maximum likelihood estimate with the key-term separation principle in (Li and Ding, 2011). Chen et al. used a gradient algorithm to identify the Hammerstein systems with continuous non-linearity (Chen et al., 2012), which only considered the single rate sampling.

There have been factors like data acquisition and transmission, frequency characteristics and hardware constraints, which can cause that the inputs and outputs are asynchronously measured with non-uniform sampling intervals.

There exists some work on the non-uniformly sampled-data systems, e.g., the related problems including modeling and estimation have been suggested in (Ding et al., 2009). The work analyzed the controllability and observability of the non-uniformly sampled systems and discussed the method for reconstructing continuous systems from non-uniformly sampled discrete-time data. With a high dimensional parameter vector, the decomposition was used to obtain a set of sub-models to be identified and a hierarchical identification algorithm with low computation was proposed (Liu et al., 2012). (Xu, 2017) estimated the parameters of transfer functions and (Xu et al., 2018) studied the parameter estimation problem of signal modeling. The widely employed approach to identifying non-uniformly sampled Hammerstein systems is the lifting technique (Ding and Lin, 2014), which uses the non-uniform sampling input-output data to build the lifted transfer function models or the lifted state-space models. Many estimation algorithms have been presented for the lifted models, e.g., a lifted transfer function model was obtained for asynchronous non-uniformly sampled-data systems in (Xie et al., 2017). (Zhou et al., 2017) presented a hierarchical recursive algorithm for asynchronous sampling Hammerstein systems by the least squares principle.

However, for Hammerstein systems with irregular updating and sampling intervals, the traditional lifted state-space models involve the problem of causality constraints, and lifted transfer function models include a larger number of parameters, resulting in increased computation complexity in the identification procedure. An input-output representation, as a novel identification model, was originally proposed for linear time-invariant processes with periodic non-uniform sampling by introducing a time-varying backward shift operator in (Xie et al., 2016). The presented model involves fewer parameters and has a more concise structure than lifted models. (Xie and Yang, 2017) applied this model to non-uniformly sampled Hammerstein systems with synchronised input and output data. Following the work in (Xie et al., 2016), this paper extends the novel model to a non-uniformly sampled Hammerstein system with saturation and dead-zone, and builds an input-output identification model for asynchronous input and output data. Moreover, decreasing the number of estimated parameters by the key-term separation principle (Li and Ding, 2011) and replacing unmeasurable internal variables with their corresponding estimates by the auxiliary model idea (Xie and Yang, 2017), the gradient-based iterative identification algorithm is further suggested to identify the model parameters.

This paper is organized as follows. A new identification model is derived for non-uniformly sampled Hammerstein systems with saturation and dead-zone in Section 2. Section 3 provides a forgetting factor stochastic gradient algorithm and a gradient-based iterative (GI) algorithm to identify the model parameters. Section 4 offers a simulation example and a two-tank system to confirm that the GI algorithm proposed works effectively and performs better than the forgetting factor stochastic gradient algorithm. Last but not least, some conclusions are made in Section 5.

2. THE SYSTEM DESCRIPTION AND MODEL DERIVATION

Consider the input-nonlinear systems (*i.e.*, Hammerstein systems) with non-uniform sampling as shown in Fig. 1. The nonlinear part $f(\cdot)$ is followed by the linear SISO continuous-time process P. The zero-order hold H_τ and the non-uniform sampler $S_{\tau+\Delta}$ generate non-uniformly sampled input-output data. The zero-order hold H_τ has the non-uniform updating intervals $\tau_i (i = 1,2,\ldots,r.)$, producing the continuous-time input $u(t)$ of $f(\cdot)$. The input data is updated r times in each acquisition period T, i.e., $t_0 = 0$, $t_i = \tau_1 + \tau_2 + \cdots + \tau_i$ for $i = 1,2, \ldots, r$, $T = \tau_1 + \tau_2 + \cdots + \tau_r$. The output $y(t)$ of P is sampled by the non-uniform sampler $S_{\tau+\Delta}$, generating a discrete-time output sequence $y(kT + t_i + d_i)(0 \le d_i < \tau_{i+1}$ for $i = 0,1,2,\ldots,r-1.)$ where d_i denotes the time lag compared with the input sampling instants. When $d_i = 0$, the systems turn into synchronous ones.

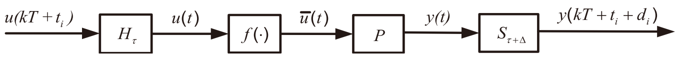

Fig. 1. The schematic of non-uniformly sampled Hammerstein systems.

Fig. 2 shows the updating and sampling pattern of the non-uniform zero-order hold and sampler. During acquisition period T, the input is non-uniformly updated r times with intervals $\{\tau_1, \tau_2, \ldots, \tau_r\}$ at time instants $\{t_0, t_1, \ldots t_r\}$, where $t_r = T$; the output is sampled at time instants $t_0 + d_0, t_1 + d_1, \ldots t_{r-1} + d_{r-1}$, where $d_0, d_1, \ldots d_{r-1}$ denote time-lag between the output and the input. Assuming that the sampling intervals $\{\tau_1, \tau_2, \cdots, \tau_r; d_0, d_1, \cdots, d_{r-1}\}$ are known, the corresponding input and output data can be known. To simplify expression, use the subscript Δ to indicate the time-lag and introduce the following notations: $u_i(k) \coloneqq u(kT + t_i)$, $\overline{u}_i(k) \coloneqq \overline{u}(kT + t_i)$, $y_{i+\Delta}(k) \coloneqq y(kT + t_i + d_i)$, where the symbol "$A \coloneqq B$" denotes that "$B$" is marked as "$A$". With the non-uniform zero-order hold H_τ, $u(t)$ and $\overline{u}(t)$ can be described as $u(t) = u(kT + t_i) = u_i(k)$, $\overline{u}(t) = \overline{u}(kT + t_i) = \overline{u}_i(k)$, $t \in (kT + t_i, kT + t_{i+1})$.

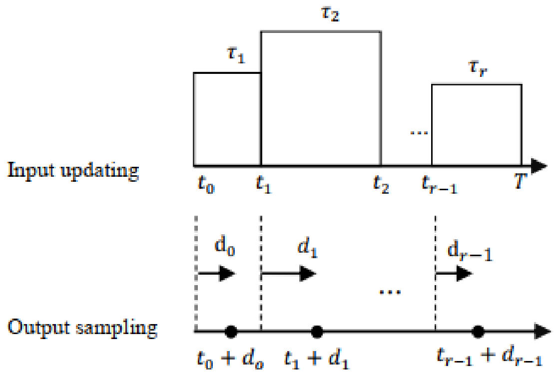

Fig. 2. The asynchronous non-uniform updating and sampling pattern.

The nonlinear block $f(\cdot)$ in Fig. 3 includes a saturation and dead-zone, which have the following expression,

$$\overline{u}(t) = \begin{cases} m_2(l_2 - l_1), & u(t) \le l_2, \\ m_2[u(t) - l_1], & l_2 < u(t) < l_1, \\ 0, & l_1 \le u(t) \le r_1, \\ m_1[u(t) - r_1], & r_1 < u(t) < r_2, \\ m_1(r_2 - r_1), & r_2 \le u(t), \end{cases} \tag{1}$$

where m_1 and m_2 $(m_1, m_2 > 0)$, r_1 and l_1, r_2 and l_2 $(r_2 > r_1, l_2 < l_1)$ denote the corresponding segment slopes, dead-zone points and saturation points, respectively.

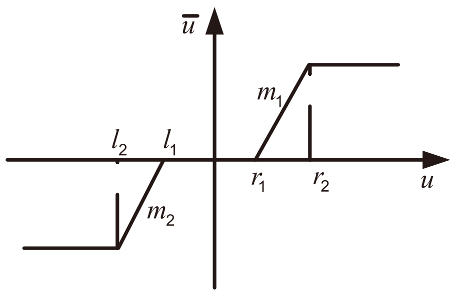

Fig. 3. The saturation and dead-zone nonlinearities.

To transform the piecewise expression into an analytic function, define a switching function (Chen et al., 2012),

$$h[u(t)] = \begin{cases} 1, & \text{if } u(t) \le 0, \\ 0, & \text{if } u(t) > 0. \end{cases}$$

Substituting it into (1), $\bar{u}(t)$ at the sampling instant $kT + t_i$ can be rewritten as

$$\begin{aligned} \bar{u}_i(k) =& m_1(r_2 - r_1)h[r_2 - u_i(k)] + m_2(l_2 - l_1)h[u_i(k) - l_2] \\ &+ m_1 h[r_1 - u_i(k)]h[u_i(k) - r_2]u_i(k) \\ &- m_1 r_1 h[r_1 - u_i(k)]h[u_i(k) - r_2] \\ &+ m_2 h[l_2 - u_i(k)]h[u_i(k) - l_1]u_i(k) \\ &- m_2 l_1 h[l_2 - u_i(k)]h[u_i(k) - l_1]. \end{aligned} \tag{2}$$

Suppose that the linear part P can be depicted by the following state space representation:

$$\begin{cases} \dot{\boldsymbol{x}}(t) = \boldsymbol{A}\boldsymbol{x}(t) + \boldsymbol{b}\bar{u}(t), \\ y(t) = \boldsymbol{c}^T\boldsymbol{x}(t) + d\bar{u}(t), \end{cases} \tag{3}$$

where $\boldsymbol{A}$ is a constant matrix with appropriate dimensions, $\boldsymbol{b}$ and $\boldsymbol{c}$ are constant vectors with appropriate dimensions, and d is a constant scalar, $\boldsymbol{x}(t) \in \mathbb{R}^n$ is the state vector, $\bar{u}(t)$ and $y(t)$ are the continuous-time process input and output, respectively.

Recent study showed that for the class of non-uniformly sampled linear systems described above using the state space representation, the output $y_{i+\Delta}(k)$ at the non-uniform sampling time $kT + t_i + d_i$ can be fully described with its previous $n+1$ non-uniformly updated inputs $\bar{u}_i(k), \bar{u}_{i-1}(k-1), \ldots, \bar{u}_{i-n}(k-n)$ and n non-uniform sampling outputs $y_{i-1+\Delta}(k-1)$, $y_{i-2+\Delta}(k-2)$, … , $y_{i-n+\Delta}(k-n)$ (Xie et al., 2016). Extending this novel idea to deal with the Hammerstein system with non-uniform sampling intervals in Fig. 1, the linear block represented by the state space model can be converted to the following input-output representation,

$$\begin{aligned} y_{i+\Delta}(k) =& -a_{i,1}y_{i-1+\Delta}(k) - a_{i,2}y_{i-2+\Delta}(k) - \cdots - \\ & a_{i,n}y_{i-n+\Delta}(k) + b_{i,0}\bar{u}_i(k) + b_{i,1}\bar{u}_{i-1}(k) + \cdots + \\ & b_{i,n}\bar{u}_{i-n}(k), \end{aligned} \tag{4}$$

where $a_{i,j}$ and $b_{i,j} (i = 0,1,2, \ldots, r-1; j = 1,2, \ldots, n)$ only depend on the coefficient matrices of the state space model, *i.e.*, $\boldsymbol{A}$, $\boldsymbol{b}$, $\boldsymbol{c}$ and d.

Notably, all the parameters $b_{i,j}$ are combined with $\bar{u}_{i-j}(k)$, so any pair of $\alpha\bar{u}_{i-j}(k)$ and $b_{i,j}/\alpha$ will produce the same output for the model in (4) if α is a nonzero constant. In order to normalize system parameters for identification, let the first coefficient of the key-term $\bar{u}_i(k)$ be 1, *i.e.*, $b_{i,0} = 1$. Then, substituting $\bar{u}_i(k)$ in (2) into (4) yields,

$$\begin{aligned} y_{i+\Delta}(k) =& m_1(r_2 - r_1)h[r_2 - u_i(k)] + \\ & m_2(l_2 - l_1)h[u_i(k) - l_2] + \\ & m_1 h[r_1 - u_i(k)]h[u_i(k) - r_2]u_i(k) - \\ & m_1 r_1 h[r_1 - u_i(k)]h[u_i(k) - r_2] + \\ & m_2 h[l_2 - u_i(k)]h[u_i(k) - l_1]u_i(k) - \\ & m_2 l_1 h[l_2 - u_i(k)]h[u_i(k) - l_1] - a_{i,1}y_{i-1+\Delta}(k) - \\ & a_{i,2}y_{i-2+\Delta}(k) - \cdots - a_{i,n}y_{i-n+\Delta}(k) + \\ & b_{i,1}\bar{u}_{i-1}(k) + \cdots + b_{i,n}\bar{u}_{i-n}(k). \end{aligned} \tag{5}$$

The information vector $\boldsymbol{\varphi}_i(k)$ and parameter vector $\boldsymbol{\theta}_i(k)$ are defined as

$$\begin{aligned} \boldsymbol{\varphi}_i(k) := & [h[r_2 - u_i(k)], h[u_i(k) - l_2], \\ & h[r_1 - u_i(k)]h[u_i(k) - r_2]u_i(k), \\ & -h[r_1 - u_i(k)]h[u_i(k) - r_2], \\ & h[l_2 - u_i(k)]h[u_i(k) - l_1]u_i(k), \\ & -h[l_2 - u_i(k)]h[u_i(k) - l_1], -y_{i-1+\Delta}(k), \\ & -y_{i-2+\Delta}(k), \ldots, -y_{i-n+\Delta}(k), \bar{u}_{i-1}(k), \\ & \bar{u}_{i-2}(k), \ldots, \bar{u}_{i-n}(k)]^{\mathrm{T}} \in \mathbb{R}^{2n+6}, \end{aligned} \tag{6}$$

$$\begin{aligned} \boldsymbol{\theta}_i := & [m_1(r_2 - r_1), m_2(l_2 - l_1), m_1, m_1 r_1, m_2, m_2 l_1, \\ & a_{i,1}, a_{i,2}, \ldots, a_{i,n}, b_{i,1}, b_{i,2}, \ldots, b_{i,n}]^{\mathrm{T}} \in \mathbb{R}^{2n+6}. \end{aligned} \tag{7}$$

Therefore, the system model can be derived as

$$y_{i+\Delta}(k) = \boldsymbol{\varphi}_i^{\mathrm{T}}(k)\boldsymbol{\theta}_i(k).$$

From (5), the system with the white noise $v_{i+\Delta}(k)$ can be denoted in matrix form

$$y_{i+\Delta}(k) = \boldsymbol{\varphi}_i^{\mathrm{T}}(k)\boldsymbol{\theta}_i(k) + v_{i+\Delta}(k). \tag{8}$$

3. THE IDENTIFICATION ALGORITHMS

In the first subsection, a forgetting factor stochastic gradient algorithm is presented for above model. To make better use of system data and achieve higher estimation accuracy, the second subsection will develop a GI identification algorithm to identify the considered system.

3.1 The auxiliary model-based forgetting factor stochastic gradient identification algorithm

A criterion function is defined as

$$J_1(\boldsymbol{\theta}_i) := [y_{i+\Delta}(k) - \boldsymbol{\varphi}_i^{\mathrm{T}}(k)\boldsymbol{\theta}_i(k)]^2,$$

minimizing it and a stochastic gradient (SG) algorithm is derived:

$$\hat{\boldsymbol{\theta}}_i(k) = \hat{\boldsymbol{\theta}}_i(k-1) + \frac{\boldsymbol{\varphi}_i(k)}{R(k)}\left[y_{i+\Delta}(k) - \boldsymbol{\varphi}_i^{\mathrm{T}}(k)\hat{\boldsymbol{\theta}}_i(k-1)\right], \tag{9}$$

$$R(k) = R(k-1) + \|\boldsymbol{\varphi}_i(k)\|^2, \; R(0) = 1. \tag{10}$$

Because of the unknown items $\bar{u}_{i-j}(k)$ and $m_1, m_2, r_1, r_2, l_1, l_2$ in the information vector $\boldsymbol{\varphi}_i(k)$, the SG algorithm in (9)-(10) fails to identify the parameter vector $\boldsymbol{\theta}_i$. To solve this problem, replacing the immeasurable items with their previous estimates based on the auxiliary model identification idea, yields

$$\begin{aligned} \hat{\boldsymbol{\varphi}}_i(k) = & [h[\hat{r}_2(k-1) - u_i(k)], h\left[u_i(k) - \hat{l}_2(k-1)\right], \\ & h[\hat{r}_1(k-1) - u_i(k)]h[u_i(k) - \hat{r}_2(k-1)]u_i(k), \\ & -h[\hat{r}_1(k-1) - u_i(k)]h[u_i(k) - \hat{r}_2(k-1)], \\ & h\left[\hat{l}_2(k-1) - u_i(k)\right]h\left[u_i(k) - \hat{l}_1(k-1)\right]u_i(k), \\ & h\left[\hat{l}_2(k-1) - u_i(k)\right]h\left[u_i(k) - \hat{l}_1(k-1)\right], \\ & -y_{i-1+\Delta}(k), -y_{i-2+\Delta}(k), \ldots, -y_{i-n+\Delta}(k), \\ & \hat{\bar{u}}_{i-1}(k-1), \hat{\bar{u}}_{i-2}(k-1), \ldots, \hat{\bar{u}}_{i-n}(k-1)]^{\mathrm{T}} \in \mathbb{R}^{2n+6}. \end{aligned}$$

Replacing unknown m_1, m_2, r_1, r_2, l_1 and l_2 with their estimates in (2), the estimate of $\bar{u}_i(k)$ can be calculated by

$$\begin{aligned}\hat{u}_i(k) = {} & \hat{m}_1(k)[\hat{r}_2(k)-\hat{r}_1(k)]h[\hat{r}_2(k)-u_i(k)] + \\ & \hat{m}_2(k)[\hat{l}_2(k)-\hat{l}_1(k)]h[u_i(k)-\hat{l}_2(k)] + \\ & \hat{m}_1(k)h[\hat{r}_1(k)-u_i(k)]h[u_i(k)-\hat{r}_2(k)]u_i(k) - \\ & \hat{m}_1(k)\hat{r}_1(k)h[\hat{r}_1(k)-u_i(k)]h[u_i(k)-\hat{r}_2(k)] + \\ & \hat{m}_2(k)h[\hat{l}_2(k)-u_i(k)]h[u_i(k)-\hat{l}_1(k)]u_i(k) - \\ & \hat{m}_2(k)\hat{l}_1(k)h[\hat{l}_2(k)-u_i(k)]h[u_i(k)-\hat{l}_1(k)].\end{aligned}$$

To increase the convergence rate, a parameter λ called the forgetting factor is introduced into the SG algorithm. Therefore, the auxiliary model based forgetting factor stochastic gradient (AM-FSG) algorithm for estimating the parameters $\boldsymbol{\theta}_i$ is deduced as:

$$\begin{aligned}\hat{\boldsymbol{\varphi}}_i(k) = {} & [h[\hat{r}_2(k-1)-u_i(k)],\ h[u_i(k)-\hat{l}_2(k-1)], \\ & h[\hat{r}_1(k-1)-u_i(k)]h[u_i(k)-\hat{r}_2(k-1)]u_i(k), \\ & -h[\hat{r}_1(k-1)-u_i(k)]h[u_i(k)-\hat{r}_2(k-1)], \\ & h[\hat{l}_2(k-1)-u_i(k)]h[u_i(k)-\hat{l}_1(k-1)]u_i(k), \\ & h[\hat{l}_2(k-1)-u_i(k)]h[u_i(k)-\hat{l}_1(k-1)], \\ & -y_{i-1+\Delta}(k),\ -y_{i-2+\Delta}(k),\ \ldots,\ -y_{i-n+\Delta}(k), \\ & \hat{\bar{u}}_{i-1}(k-1), \hat{\bar{u}}_{i-2}(k-1),\ \ldots, \hat{\bar{u}}_{i-n}(k-1)]^{\mathrm{T}}, \quad (11)\end{aligned}$$

$$R(k) = \lambda R(k-1) + \|\hat{\boldsymbol{\varphi}}_i(k)\|^2, 0 \le \lambda \le 1, R(0) = 1, \quad (12)$$

$$\hat{\boldsymbol{\theta}}_i(k) = \hat{\boldsymbol{\theta}}_i(k-1) + \frac{\hat{\varphi}_i(k)}{R(k)}[y_{i+\Delta}(k) - \hat{\boldsymbol{\varphi}}_i^{\mathrm{T}}(k)\hat{\boldsymbol{\theta}}_i(k-1)], \quad (13)$$

$$\begin{aligned}\hat{\boldsymbol{\theta}}_i(k) = {} & [\hat{m}_1(k)[\hat{r}_2(k)-\hat{r}_1(k)], \hat{m}_2(k)[\hat{l}_2(k)-\hat{l}_1(k)], \\ & \hat{m}_1(k), \hat{m}_1(k)\hat{r}_1(k), \hat{m}_2(k), \hat{m}_2(k)\hat{l}_1(k), \hat{a}_{i,1}(k), \\ & \hat{a}_{i,2}(k), \ldots, \hat{a}_{i,n}(k), \hat{b}_{i,1}(k), \hat{b}_{i,2}(k), \ldots, \hat{b}_{i,n}(k)]^{\mathrm{T}}, \quad (14)\end{aligned}$$

$$\hat{m}_1(k) = \hat{\boldsymbol{\theta}}_{i,3}(k),\ \hat{m}_2(k) = \hat{\boldsymbol{\theta}}_{i,5}(k), \quad (15)$$

$$\hat{r}_1(k) = \frac{\hat{\boldsymbol{\theta}}_{i,4}(k)}{\hat{m}_1(k)},\ \hat{r}_2(k) = \frac{\hat{\boldsymbol{\theta}}_{i,1}(k)}{\hat{m}_1(k)} + \hat{r}_1(k), \quad (16)$$

$$\hat{l}_1(k) = \frac{\hat{\boldsymbol{\theta}}_i(k)(6)}{\hat{m}_2(k)},\ \hat{l}_2(k) = \frac{\hat{\boldsymbol{\theta}}_i(k)(2)}{\hat{m}_2(k)} + \hat{l}_1(k), \quad (17)$$

$$\begin{aligned}\hat{\bar{u}}_i(k) = {} & \hat{m}_1(k)[\hat{r}_2(k)-\hat{r}_1(k)]h[\hat{r}_2(k)-u_i(k)] + \\ & \hat{m}_2(k)[\hat{l}_2(k)-\hat{l}_1(k)]h[u_i(k)-\hat{l}_2(k)] + \\ & \hat{m}_1(k)h[\hat{r}_1(k)-u_i(k)]h[u_i(k)-\hat{r}_2(k)]u_i(k) - \\ & \hat{m}_1(k)\hat{r}_1(k)h[\hat{r}_1(k)-u_i(k)]h[u_i(k)-\hat{r}_2(k)] + \\ & \hat{m}_2(k)h[\hat{l}_2(k)-u_i(k)]h[u_i(k)-\hat{l}_1(k)]u_i(k) - \\ & \hat{m}_2(k)\hat{l}_1(k)h[\hat{l}_2(k)-u_i(k)]h[u_i(k)-\hat{l}_1(k)]. \quad (18)\end{aligned}$$

where $\hat{\boldsymbol{\theta}}_{i,j}(k)$ denotes the jth element of parameter vector $\hat{\boldsymbol{\theta}}_i(k)$.

Then the identification steps of the AM-FSG algorithm in (11) -(18) are summarized as shown in Fig. 4.

In Fig. 4, the initial values: $\boldsymbol{\theta}_i(0) = \mathbf{1}_{2n+6}/p_0$ ($\mathbf{1}_{2n+6}$ stands for an $2n+6$-dimensional column vector whose elements are 1.), $p_0 = 10^6$, $\hat{\bar{u}}_i(0) = 1/p_0$, $R(0) = 1$.

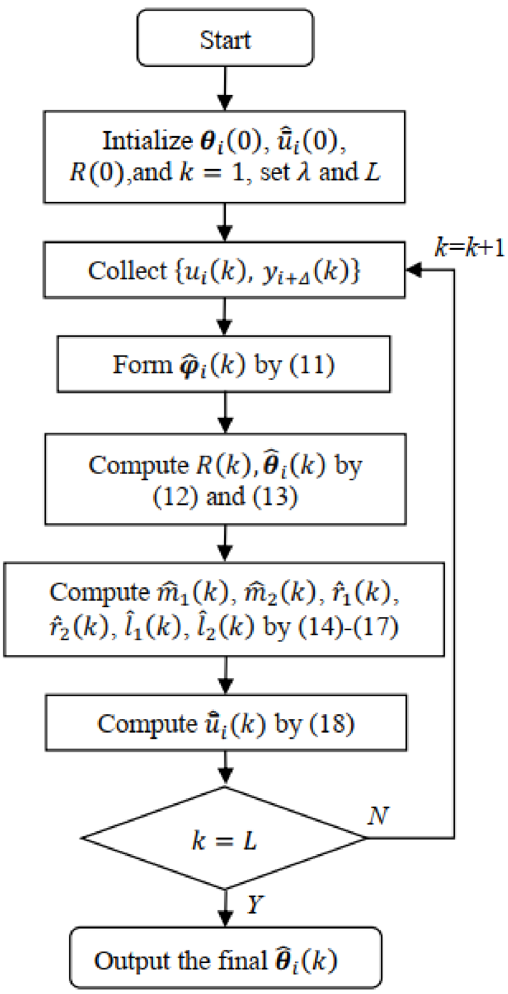

Fig. 4. The flowchart of the AM-FSG algorithm.

3.2 The gradient based iterative identification algorithm

This section gives a GI algorithm for identifying the model in (8) by introducing the negative gradient search principle. The unknown $\bar{u}_{i-j}(k)$ and m_1, m_2, r_1, r_2, l_1, l_2 in the information vector $\boldsymbol{\varphi}_i(k)$ are replaced with their estimates according to the auxiliary model identification idea.

Firstly, the stacked output vector $\boldsymbol{Y}(L)$, stacked information matrix $\boldsymbol{\Phi}(L)$ and white noise vector $\boldsymbol{V}(L)$ are defined as follows:

$$\boldsymbol{Y}_{i+\Delta}(L) = \begin{bmatrix} y_{i+\Delta}(L) \\ y_{i+\Delta}(L-1) \\ \vdots \\ y_{i+\Delta}(1) \end{bmatrix} \in \mathbb{R}^L,$$

$$\boldsymbol{\Phi}_i(L) = \begin{bmatrix} \boldsymbol{\varphi}_i^{\mathrm{T}}(L) \\ \boldsymbol{\varphi}_i^{\mathrm{T}}(L-1) \\ \vdots \\ \boldsymbol{\varphi}_i^{\mathrm{T}}(1) \end{bmatrix} \in \mathbb{R}^{L\times(2n+6)}, \quad (19)$$

$$\boldsymbol{V}_{i+\Delta}(L) = \begin{bmatrix} v_{i+\Delta}(L) \\ v_{i+\Delta}(L-1) \\ \vdots \\ v_{i+\Delta}(1) \end{bmatrix} \in \mathbb{R}^L,$$

where L means the data length. From (8) and (19), the Hammerstein system equation can be described by the matrix form:

$$\boldsymbol{Y}_{i+\Delta}(L) = \boldsymbol{\Phi}_i(L)\boldsymbol{\theta}_i + \boldsymbol{V}_{i+\Delta}(L).$$

Define the criterion function:

$$J_2(\boldsymbol{\theta}_i) := \frac{1}{2}\|\boldsymbol{Y}_{i+\Delta}(L) - \boldsymbol{\Phi}_i(L)\boldsymbol{\theta}_i\|^2 \tag{20}$$

Taking the gradient of $J_2(\boldsymbol{\theta}_i)$ with respect to $\boldsymbol{\theta}_i$ yields

$$\mathrm{grad}[J_2(\boldsymbol{\theta}_i)] = \frac{\partial J_2(\boldsymbol{\theta}_i)}{\partial \boldsymbol{\theta}_i} = -[\boldsymbol{\Phi}_i(L)]^{\mathrm{T}}[\boldsymbol{Y}_{i+\Delta}(L) - \boldsymbol{\Phi}_i(L)\boldsymbol{\theta}_i].$$

Minimizing the criterion function in (20) by the negative gradient search principle (Ding et al., 2019), the GI algorithm is derived:

$$\begin{aligned}\hat{\boldsymbol{\theta}}_i^p &= \hat{\boldsymbol{\theta}}_i^{p-1} - \mu_p \mathrm{grad}[J_2(\hat{\boldsymbol{\theta}}_i^{p-1})] \\ &= \hat{\boldsymbol{\theta}}_i^{p-1} + \mu_p[\boldsymbol{\Phi}_i^p(L)]^{\mathrm{T}}[\boldsymbol{Y}_{i+\Delta}(L) - \boldsymbol{\Phi}_i^p(L)\hat{\boldsymbol{\theta}}_i^{p-1}],\end{aligned} \tag{21}$$

where $p = 1,2,3,\cdots$ and μ_p denote the iteration variable and the iterative step-size, respectively, $\hat{\boldsymbol{\theta}}_i^p$ is the estimate of $\boldsymbol{\theta}_i$ at iteration p.

Due to the unknown item $\bar{u}_{i-j}(k)$ and unknown parameters $m_1, m_2, r_1, r_2, l_1, l_2$ in $\boldsymbol{\varphi}_i(k)$, the iterative algorithm fails to identify system parameters. Using the previous iterative estimates to replace the unknown item and unknown parameters, respectively, a GI identification algorithm can be deduced as

$$\hat{\boldsymbol{\theta}}_i^p = \hat{\boldsymbol{\theta}}_i^{p-1} + \mu_p[\hat{\boldsymbol{\Phi}}_i^p(L)]^{\mathrm{T}}[\boldsymbol{Y}_{i+\Delta}(L) - \hat{\boldsymbol{\Phi}}_i^p(L)\hat{\boldsymbol{\theta}}_i^{p-1}], \tag{22}$$

$$\boldsymbol{Y}_{i+\Delta}(L) = [y_{i+\Delta}(L), y_{i+\Delta}(L-1), \cdots, y_{i+\Delta}(1)]^{\mathrm{T}}, \tag{23}$$

$$\hat{\boldsymbol{\Phi}}_i^p(L) = [\hat{\boldsymbol{\varphi}}_i^p(L), \hat{\boldsymbol{\varphi}}_i^p(L-1), \cdots, \hat{\boldsymbol{\varphi}}_i^p(1)]^{\mathrm{T}}, \tag{24}$$

$$\begin{aligned}\hat{\boldsymbol{\varphi}}_i^p(k) := [&h[\hat{r}_2^{p-1} - u_i(k)], h[u_i(k) - \hat{l}_2^{p-1}], \\ &h[\hat{r}_1^{p-1} - u_i(k)]h[u_i(k) - \hat{r}_2^{p-1}]u_i(k), \\ &-h[\hat{r}_1^{p-1} - u_i(k)]h[u_i(k) - \hat{r}_2^{p-1}], \\ &h[\hat{l}_2^{p-1} - u_i(k)]h[u_i(k) - \hat{l}_1^{p-1}]u_i(k), \\ &-h[\hat{l}_2^{p-1} - u_i(k)]h[u_i(k) - \hat{l}_1^{p-1}], -y_{i-1+\Delta}(k), \\ &-y_{i-2+\Delta}(k), \cdots, -y_{i-n+\Delta}(k), \hat{\bar{u}}_{i-1}^{p-1}(k), \hat{\bar{u}}_{i-2}^{p-1}(k), \\ &\cdots, \hat{\bar{u}}_{i-n}^{p-1}(k)]^{\mathrm{T}} \in \mathbb{R}^{2n+6},\end{aligned} \tag{25}$$

$$\begin{aligned}\hat{\bar{u}}_i^p(k) = \,&\hat{m}_1^p(\hat{r}_2^p - \hat{r}_1^p)h[\hat{r}_2^p - u_i(k)] + \\ &\hat{m}_2^p(\hat{l}_2^p - \hat{l}_1^p)h[u_i(k) - \hat{l}_2^p] + \\ &\hat{m}_1^p h[\hat{r}_1^p - u_i(k)]h[u_i(k) - \hat{r}_2^p]u_i(k) - \\ &\hat{m}_1^p\hat{r}_1^p h[\hat{r}_1^p - u_i(k)]h[u_i(k) - \hat{r}_2^p] + \\ &\hat{m}_2^p h[\hat{l}_2^p - u_i(k)]h[u_i(k) - \hat{l}_1^p]u_i(k) - \\ &\hat{m}_2^p\hat{l}_1^p h[\hat{l}_2^p - u_i(k)]h[u_i(k) - \hat{l}_1^p],\end{aligned} \tag{26}$$

$$\begin{aligned}\hat{\boldsymbol{\theta}}_i^p = [&\hat{m}_1^p[\hat{r}_2^p - \hat{r}_1^p], \hat{m}_2^p[\hat{l}_2^p - \hat{l}_1^p], \hat{m}_1^p, \hat{m}_1^p\hat{r}_1^p, \hat{m}_2^p, \hat{m}_2^p\hat{l}_1^p, \\ &\hat{a}_{i,1}^p, \hat{a}_{i,2}^p, \ldots, \hat{a}_{i,n}^p, \hat{b}_{i,1}^p, \hat{b}_{i,2}^p, \ldots, \hat{b}_{i,n}^p]^{\mathrm{T}},\end{aligned} \tag{27}$$

$$\hat{m}_1^p = \hat{\boldsymbol{\theta}}_i^p(3),\ \hat{m}_2^p = \hat{\boldsymbol{\theta}}_i^p(5), \tag{28}$$

$$\hat{r}_1^p = \frac{\hat{\boldsymbol{\theta}}_i^p(4)}{\hat{m}_1^p},\ \hat{r}_2^p = \frac{\hat{\boldsymbol{\theta}}_i^p(1)}{\hat{m}_1^p} + \hat{r}_1^p, \tag{29}$$

$$\hat{l}_1^p = \frac{\hat{\boldsymbol{\theta}}_i^p(6)}{\hat{m}_2^p},\ \hat{l}_2^p = \frac{\hat{\boldsymbol{\theta}}_i^p(2)}{\hat{m}_2^p} + \hat{l}_1^p, \tag{30}$$

$$0 < \mu_p \le \frac{2}{\lambda_{\max}\left\{[\hat{\boldsymbol{\Phi}}_i^p(L)]^{\mathrm{T}}\hat{\boldsymbol{\Phi}}_i^p(L)\right\}}. \tag{31}$$

where $\lambda_{max}\{X\}$ represents the maximum eigenvalue of the nonnegative definite matrix X. The identification steps of the GI algorithm are shown in Fig. 5.

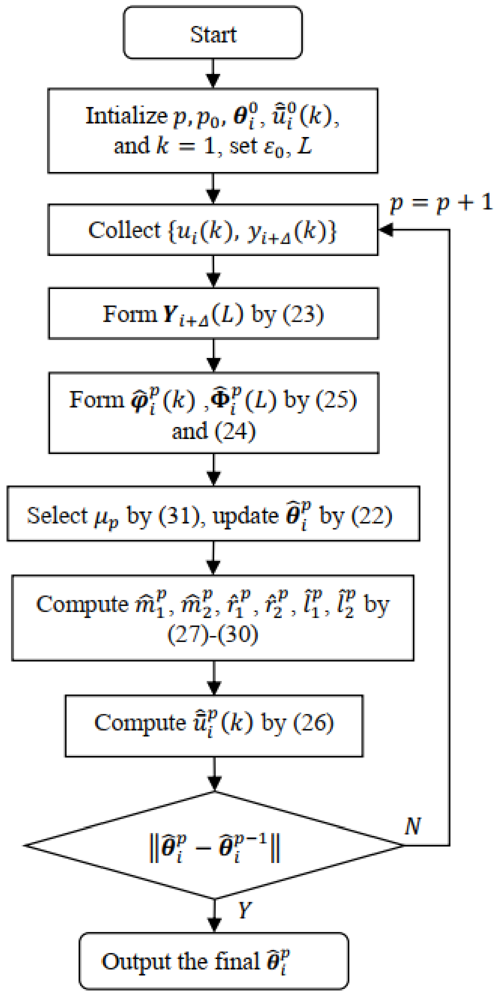

Fig. 5. The flowchart of proposed method.

In Fig.5, the initial values $p = 1$, $\boldsymbol{\theta}_i^0 = \mathbf{1}_{2n+6}/p_0$, $p_0 = 10^6$, $\hat{\bar{u}}_i^0(k) = 1/p_0$. The parameter μ_p only needs to be within the range expressed by (31), and the maximum value of μ_p is selected in this paper.

4. EXAMPLES

In this section, a numerical Hammerstein system and a continuous two-tank system with saturation and dead-zone nonlinearity are used to show the effectiveness of the GI algorithm.

4.1 Numerical example

To demonstrate how the proposed algorithms work and make a comparison between them, this section gives a numerical example, which has a Hammerstein system in state-space form as following:

$$\begin{cases}\dot{\boldsymbol{x}}(t) &= \begin{bmatrix}-0.35 & -0.045\\ 1 & 0\end{bmatrix}\boldsymbol{x}(t) + \begin{bmatrix}0.03\\ 0\end{bmatrix}\bar{u}(t),\\ y(t) &= [0, 0.035]\boldsymbol{x}(t) + 0.035\bar{u}(t).\end{cases}$$

Convert to the following input-output representation with non-uniform sampling times $r = 2$:

$$\begin{aligned}y_{i+\Delta}(k) =& -a_{i,1}y_{i-1+\Delta}(k) - a_{i,2}y_{i-2+\Delta}(k) +\\ & \bar{u}_i(k) + b_{i,1}\bar{u}_{i-1}(k) + b_{i,2}\bar{u}_{i-2}(k) +\\ & \mathrm{v}_{i+\Delta}(k), i = 0, 1,\end{aligned}$$

where

$$\boldsymbol{a}_0 = \left[a_{0,1},\ a_{0,2}\right]^{\mathrm{T}} = [-0.26456, 0.044]^{\mathrm{T}},$$

$$\boldsymbol{a}_1 = [a_{1,1},\ a_{1,2}]^{\mathrm{T}} = [-0.15513, 0.04564]^{\mathrm{T}},$$

$$\boldsymbol{b}_0 = [b_{0,1},\ b_{0,2}]^{\mathrm{T}} = [0.03926, 0.00388]^{\mathrm{T}},$$

$$\boldsymbol{b}_1 = [b_{1,1},\ b_{1,2}]^{\mathrm{T}} = [0.04229, 0.00642]^{\mathrm{T}}.$$

The nonlinearity is shown in Fig.3, with

$$\begin{aligned}\boldsymbol{\omega} &= [m_1, m_2, r_1,\ r_2,\ l_1, l_2]^{\mathrm{T}}\\ &= [0.44, 0.1, 0.04, 0.54, -0.15, -0.75]^{\mathrm{T}}\end{aligned}$$

Assume $T = 13s$, $\tau_1 = 6s$, $\tau_2 = 7s$ and $d_0 = 3.5s$, $d_1 = 4s$. The system is assumed to have a periodic non-uniform updating and sampling pattern as illustrated in Fig.6. The input $\{u_i(k), i = 0,1\}$ is a random signal sequence with zero mean and unit variance, while the noise $\{v_{i+\Delta}(k), i = 0, 1\}$ is white Gaussian with zero mean and constant variance $\sigma^2 = 0.2^2$. The estimation error is defined as

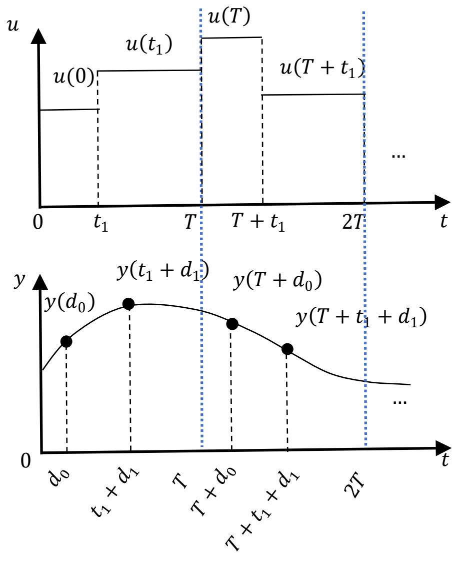

Fig. 6. The sampling pattern with asynchronous input-output data.

$$\varepsilon := \frac{\sum_{i=0}^{1}\left[\|\hat{\boldsymbol{a}}_i - \boldsymbol{a}_i\|^2 + \left\|\hat{\boldsymbol{b}}_i - \boldsymbol{b}_i\right\|^2\right] + \|\hat{\boldsymbol{\omega}} - \boldsymbol{\omega}\|^2}{\sum_{i=0}^{1}[\|\boldsymbol{a}_i\|^2 + \|\boldsymbol{b}_i\|^2] + \|\boldsymbol{\omega}\|^2}, \qquad \text{-(32)}$$

where $\|\boldsymbol{x}\|^2$ represents the sum of the squares of the elements in the vector $\boldsymbol{x}$: $\|\boldsymbol{x}\|^2 = \sum x_i^2$. The (32) only applied when the true parameters of the model are known. In practical system identification, when the parameters of the model are unknown, it is not possible to calculate the estimation error of the parameters, but only to observe how the output values of the model track the true output of the system.

Apply the AM-FSG algorithm in (11)-(18) and the GI algorithm in (22)-(31) to identify the considered system. In experiments, different forgetting factor values are usually chosen to observe the estimation performance in order to obtain the optimal value. In this paper, the forgetting factor value λ is chosen as (0.99, 0.98, 0.97, 0.96). The parameter estimates and their errors of the AM-FSG algorithm with $\lambda =$ 0.99, 0.98, 0.97, 0.96 are shown in Table 1, and the corresponding errors are plotted in Fig.7. With the data length $L = 5000$, the estimates and errors of the GI algorithm are shown in Table 2, and the corresponding estimation error ε versus iteration variable p is plotted in Fig.8. To study the identification performance of the proposed algorithm against the output noise, Monte-Carlo simulation is conducted for the numerical example by randomly changing the input sequences. Fig.9 shows simulation result which is the mean estimation error of the GI algorithm.

Table 1. The numerical example: estimates and errors of the AM-FSG algorithm (L = 5000).

k	$\lambda = 0.99$	$\lambda = 0.98$	$\lambda = 0.97$	$\lambda = 0.96$	True values
$a_{0,1}$	-0.23805	-0.27083	-0.26446	-0.24632	-0.26456
$a_{0,2}$	0.03494	0.05586	0.03051	0.05072	0.04400
$b_{0,1}$	0.04465	0.02712	0.00729	-0.02672	0.03926
$b_{0,2}$	-0.05310	-0.12406	-0.00987	-0.04262	0.00388
$a_{1,1}$	-0.13800	-0.16666	-0.14049	-0.14027	-0.15513
$a_{1,2}$	0.04337	0.05758	0.04807	0.05501	0.04564
$b_{1,1}$	0.04161	0.02526	0.00663	-0.02974	0.04229
$b_{1,2}$	-0.06437	-0.13337	-0.03266	-0.04888	0.00642
m_1	0.23007	0.25997	0.23385	0.23992	0.44000
m_2	0.00034	0.00090	0.06945	0.05572	0.10000
r_1	-0.01828	0.05859	0.07934	0.13975	0.04000
r_2	0.94251	0.98636	1.09590	1.24970	0.54000
l_1	-10.79600	-3.09350	-0.70776	-1.99450	-0.15000
l_2	-7.24000	-7.89460	-1.61710	-2.84570	-0.75000
$\varepsilon(\%)$	6.77240	8.27360	4.93360	6.92360	

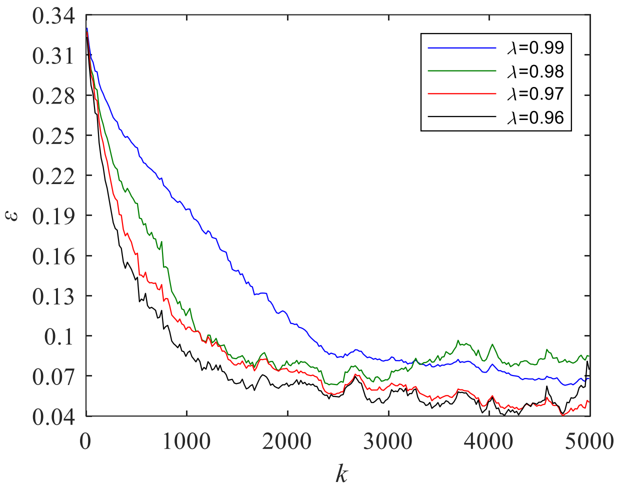

Fig. 7. The numerical example: parameter estimation error of the AM-FSG algorithm ε vs. k.

Table 2. The numerical example: estimates and errors of the GI algorithm

p	50	100	200	400	600	800	True values
$a_{0,1}$	-0.25722	-0.25622	-0.25360	-0.25250	-0.25273	-0.25275	-0.26456
$a_{0,2}$	0.02137	0.02765	0.02867	0.02981	0.03010	0.03009	0.04400
$b_{0,1}$	0.02179	0.03433	0.04629	0.04301	0.04235	0.04226	0.03926
$b_{0,2}$	-0.01425	-0.00577	0.00320	0.00326	0.00399	0.00395	0.00388
$a_{1,1}$	-0.15359	-0.14860	-0.14459	-0.14317	-0.14338	-0.14342	-0.15513
$a_{1,2}$	0.02544	0.02989	0.03098	0.03207	0.03237	0.03234	0.04564
$b_{1,1}$	0.01568	0.03265	0.04838	0.04599	0.04539	0.04534	0.04229
$b_{1,2}$	-0.01056	-0.00298	0.00530	0.00518	0.00597	0.00597	0.00642
m_1	0.21961	0.25750	0.32139	0.41632	0.44026	0.44034	0.44000
m_2	0.04157	0.04202	0.04561	0.08411	0.08400	0.08395	0.10000
r_1	-0.25733	-0.16011	-0.04062	0.05526	0.06791	0.06833	0.04000
r_2	0.73432	0.68232	0.63034	0.57481	0.55872	0.55911	0.54000
l_1	0.57935	0.49485	0.37891	-0.09063	-0.09397	-0.09642	-0.15000
l_2	-1.02560	-1.13220	-1.13200	-0.91626	-0.92013	-0.92316	-0.75000
$\varepsilon(\%)$	6.16620	4.24160	1.98760	0.17035	0.12281	0.12301	

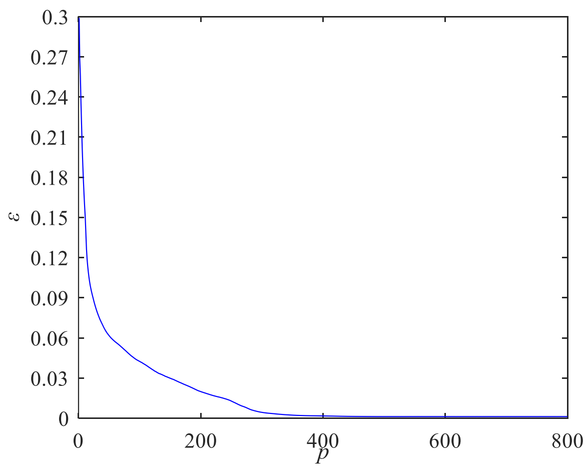

Fig. 8. The numerical example: parameter estimation error of the GI algorithm ε vs. p.

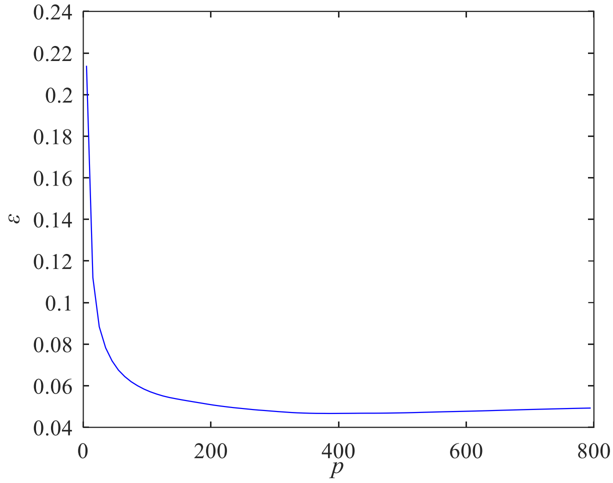

Fig. 9. The numerical example: mean estimation error of the GI algorithm ε vs. p.

From Table 1 and Fig.7, it is apparent that for the AM-FSG algorithm, its estimation error decreases as the forgetting factor λ decreases. However, some parameter estimates deviate far from the true ones. And the parameter estimates also fluctuate a lot when λ is smaller than 0.97. The results illustrate that the effectiveness of the AM-FSG algorithm for this considered non-uniform sampling Hammerstein system needs to be further improved.

For the GI algorithm, it's evident that its estimation error becomes smaller and all estimates gradually approach to their true values with the increase of iterations p, and its convergence rate is very speedy from Table 2 and Fig.8. Moreover, changing the random sequences by different random number seed (8:130), Fig.9 depicts that the mean estimation errors are fast and smooth close to the true values, which further illustrates that the GI algorithm has a smooth and good performance.

To show the evolution of parameter estimates along with the iterations p, the parameters a_0, m_1, r_2 are randomly chosen for presentation in Fig.10, and Fig.11 compares the measured output $y(t)$ with predicted output of the non-uniformly

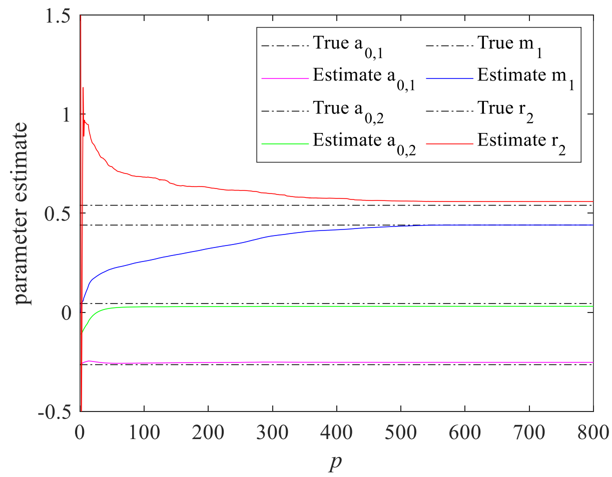

Fig. 10. The numerical example: the estimation value a_0, m_1, r_2 of the GI algorithm vs. p.

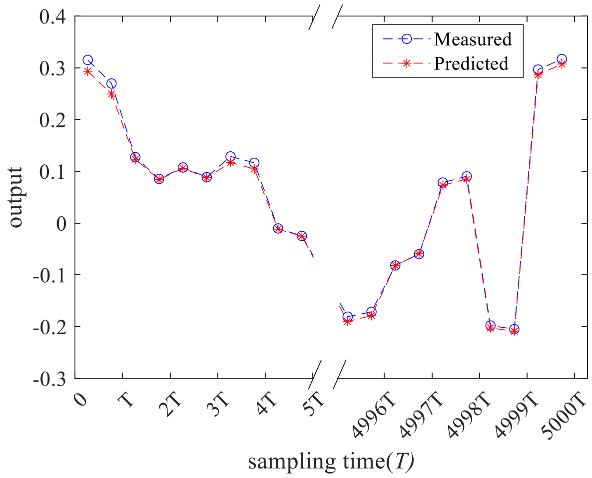

Fig. 11. The numerical example: measured output $y(t)$ and predicted output of the non-uniformly system.

system. In Fig.11, the model obtained by the proposed method can accurately track the true output, and furthermore, the differences between the predicted values of the outputs and their true measured values at the beginning and the end of the process do not have a specific meaning. As shown in Fig.10 and Fig.11, all the parameter estimates gradually converge to the true parameters, demonstrating the effectiveness of the proposed identification algorithm.

Comparing Table 1 with Table 2, the estimates of the GI algorithm are much closer to the true values than that of the AM-FSG algorithm, and have significantly smaller parameter estimation errors in the last rows in these Tables. The results validate that the proposed GI identification method has a more superior estimation accuracy.

4.2 Two-tank system

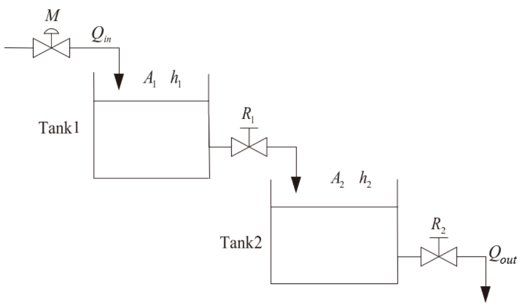

Fig. 12. Schematic diagram of two-tank system.

Consider the two-tank system shown in Fig.12. The motorized valve M may include a saturation and dead-zone characteristic, which has translation relation with that of Fig. 3. The output of the valve is zero when its input signal is not big enough to open the valve. The output of the valve may remain constant when its input changes in a small range. The insensitive phenomenon may be caused by some actuator arrearage faults and a PID control algorithm with insensitive region aimed at avoiding damage from frequent action of the actuator. Therefore, the two-tank system can be tailored as a non-uniform sampling process for system identification and algorithm testing. In Fig.12, the tanks are located on different levels, unlike those on the same level in (Changela and Kumar, 2015), which means that they have different linear resistance to flow. Referring to the derivation of the mathematical model in (Changela and Kumar, 2015), the two-tank system is modeled as a simplified and linearized model

$$A_1\frac{dh_1}{dt} = Q_{in} - c_1 h_1,$$
$$A_2\frac{dh_2}{dt} = c_1 h_1 - Q_{out},$$
$$Q_{out} = c_2 h_2,$$

where Q_{in} is the volumetric flow rate into Tank1, Q_{out} is the volumetric flow rate from Tank2; $A_1 = 1m^2$ and $A_2 = 1.2m^2$ are the cross-section areas of the two tanks respectively; $c_1 = 0.5$ and $c_2 = 0.8$ the coefficients after linearization and associated with the valves R_1 and R_2 respectively; h_1 and h_2 the liquid levels in Tank1 and Tank2 respectively.

Using Equation (5), with the non-uniform sampling times $r = 2$, the identification model of two-tank system can be deduced as

$$\begin{aligned} y_{i+\Delta}(k) = & m_1(r_2 - r_1)h[r_2 - u_i(k)] + \\ & m_2(l_2 - l_1)h[u_i(k) - l_2] + \\ & m_1 h[r_1 - u_i(k)]h[u_i(k) - r_2]u_i(k) - \\ & m_1 r_1 h[r_1 - u_i(k)]h[u_i(k) - r_2] + \\ & m_2 h[l_2 - u_i(k)]h[u_i(k) - l_1]u_i(k) - \\ & m_2 l_1 h[l_2 - u_i(k)]h[u_i(k) - l_1] - a_{i,1}y_{i-1+\Delta}(k) - \\ & a_{i,2}y_{i-2+\Delta}(k) + b_{i,1}\bar{u}_{i-1}(k) + b_{i,2}\bar{u}_{i-n}(k) + \\ & v_{i+\Delta}(k), i = 0,1, \end{aligned}$$

where the true values of the parameters $\boldsymbol{a}_i$ and $\boldsymbol{b}_i$ are as follows:

$$\boldsymbol{a}_0 = [a_{0,1}, a_{0,2}]^{\mathrm{T}} = [-0.4451, 0.0816]^{\mathrm{T}},$$
$$\boldsymbol{b}_0 = [b_{0,1}, b_{0,2}]^{\mathrm{T}} = [0.5258, 0.2648]^{\mathrm{T}},$$
$$\boldsymbol{a}_1 = [a_{1,1}, a_{1,2}]^{\mathrm{T}} = [-0.7501, 0.0320]^{\mathrm{T}},$$
$$\boldsymbol{b}_1 = [b_{1,1}, b_{1,2}]^{\mathrm{T}} = [0.2677, 0.2476]^{\mathrm{T}}.$$

The nonlinearity parameters are set as

$$\begin{aligned} \boldsymbol{\omega} &= [m_1, m_2, r_1, r_2, l_1, l_2]^{\mathrm{T}} \\ &= [0.38, 0.02, 0.8, 2.6, 0.65, 0.02]^T. \end{aligned}$$

The acquisition period is selected as $T = 5s$, $\tau_1 = 3s$, $\tau_2 = 2s$ and $d_0 = 2.5s$, $d_1 = 1.5s$. The input $\{u_i(k), i = 0,1\}$ is a random signal sequence with zero mean and unit variance, while the noise $\{v_{i+\Delta}(k), i = 0,1\}$ is white Gaussian with zero mean and constant variance $\sigma^2 = 0.2^2$. Through the simulation of the above two algorithms, the estimation errors of the GI algorithm and AM-FSG algorithm are 0.21710% and 3.3532%, respectively. The estimated parameters of the AM-FSG algorithm (λ=0.97, L=5000) and GI algorithm (p=800) are presented in Table 3.

Table 3. The two-tank system: estimates and errors of the AM-FSG algorithm (λ =0.97, L = 5000) and GI algorithm (p=800)

	AM-FSG	GI	True value
$a_{0,1}$	-0.4553	-0.4418	-0.4451
$a_{0,2}$	0.0925	0.0774	0.0816
$b_{0,1}$	0.3802	0.5049	0.5258
$b_{0,2}$	0.2073	0.2597	0.2648
$a_{1,1}$	-0.6979	-0.7347	-0.7501
$a_{1,2}$	-0.0134	0.0154	0.0320
$b_{1,1}$	0.2873	0.2635	0.2677
$b_{1,2}$	0.2651	0.2431	0.2476
m_1	0.3621	0.3971	0.3800
m_2	-0.0053	0.0219	0.0200
r_1	0.7023	0.8373	0.8000
r_2	2.6334	2.5165	2.6000
l_1	-5.0582	0.6356	0.6500
l_2	-3.9929	0.0168	0.0200
ε(%)	3.3532	0.2171	

The estimation errors of the GI algorithm are plotted in Fig.13. It reveals that the estimation error converges quickly and smoothly.

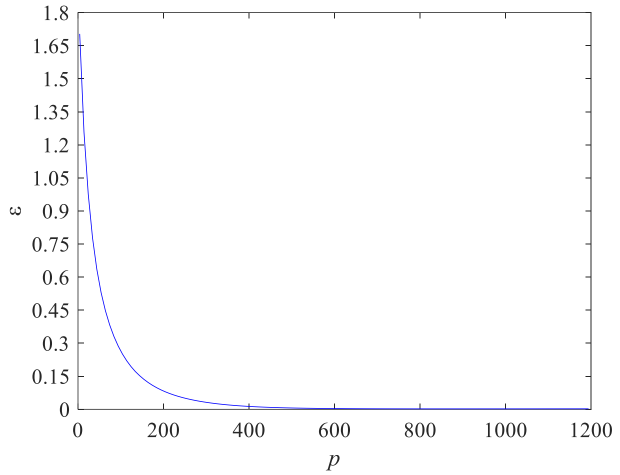

Fig. 13. The two-tank system: the estimation error of the GI algorithm ε vs. p.

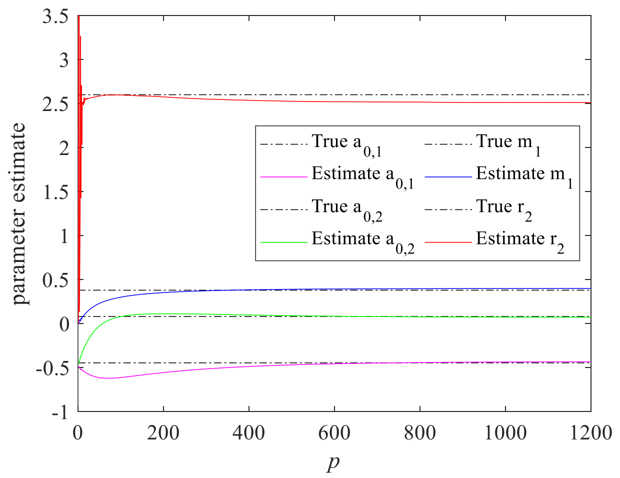

Fig. 14. The two-tank system: the estimation value a_0, m_1, r_2 of the GI algorithm vs. p.

Fig.14 and Fig.15 show the convergence of estimated parameters and the comparison between predicted output and true output respectively. The results demonstrate that the proposed GI algorithm can be used to well identify all model parameters with high accuracy.

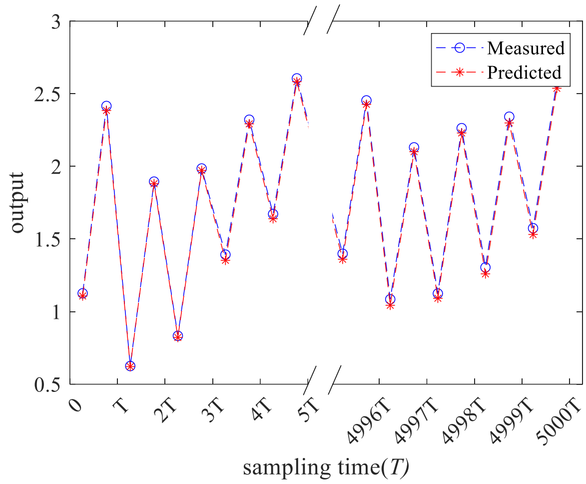

Fig. 15. The two-tank system: measured output $y(t)$and predicted output of the non-uniformly system.

5. CONCLUSIONS

We have discussed an identification method for non-uniformly sampled Hammerstein system with saturation and dead zone. By introducing the input-output expression of the n-order difference equation, a concise identification model is first established. Then, an AM-FSG algorithm is used to identify the Hammerstein models. To further improve the identification performance, a GI algorithm are proposed to identify the Hammerstein models. The GI algorithm directly estimates the parameters of the Hammerstein system using gradient search. By applying the proposed method to a numerical example and a mathematical model of the two-tank system, we have proved that the proposed method can give more accurate parameter estimations than AM-FSG algorithm. The proposed approach is applicable to tackling Hammerstein systems with other types of nonlinear blocks. It also sheds light on further research on parameter identification of non-uniformly sampled systems with more complex nonlinearities.

REFERENCES

Amer, Y., El-Sayed, A., and Ahmed, E. (2021). On controlling the nonlinear vibrations of a rectangular thin plate with time delay feedback. *Control Engineering and Applied Informatics*, 23, 40–52.

Avila, F.R., Duarte, L.T., and Biscainho, L.W. (2017). On the sparsity-based identification and compensation of hammerstein systems. *IEEE Signal Processing Letters*, 24(9), 1363–1367.

Chen, J., Wang, X., and Ding, R. (2012). Gradient based estimation algorithm for hammerstein systems with saturation and dead-zone nonlinearities. *Applied Mathematical Modelling*, 36(1), 238–243.

Changela, M., & Kumar, A. (2015). Designing a controller for two tank interacting system. *International Journal of Science and Research*, 4(5), 589-593.

Ding, F., Qiu, L., and Chen, T. (2009). Reconstruction of continuous-time systems from their non-uniformly sampled discrete-time systems. *Automatica*, 45(2), 324–332.

Ding, J. and Lin, J. (2014). Modified subspace identification for periodically non-uniformly sampled systems by using the lifting technique. *Circuits, Systems, and Signal Processing*, 33(5), 1439–1449.

Dong, Z. (2015). Model-free power-level control of mhtgrs against input saturation and dead-zone. *IEEE Transactions on Nuclear Science*, 62(6), 3297–3310.

Ding, F., Zhang, X., & Xu, L. (2019). The innovation algorithms for multivariable state - space models. *International Journal of Adaptive Control and Signal Processing*, 33(11), 1601-1618.

Gao, X., Ren, X., Zhu, C., and Zhang, C. (2015). Identification and control for hammerstein systems with hysteresis non-linearity. *IET Control Theory & Applications*, 9(13), 1935–1947.

Giri, F., Rochdi, Y., Brouri, A., and Chaoui, F.Z. (2011). Parameter identification of hammerstein systems containing backlash operators with arbitrary-shape parametric borders. *Automatica*, 47(8), 1827–1833.

Hu, Q., Ma, G., and Xie, L. (2008). Robust and adaptive variable structure output feedback control of uncertain systems with input nonlinearity. *Automatica*, 44(2), 552–559.

Ioanas, G.L. and Dragomir T.L. (2013). Common-rail pressure estimation using neuro-fuzzy architeture with local Hammerstein models. *In IEEE 8th Internation Symposium on Applied Computational Intelligence and Informatics (SACI)*, 2013: 281-286.

Li, J. and Ding, F. (2011). Maximum likelihood stochastic gradient estimation for hammerstein systems with colored noise based on the key term separation technique. *Computers & Mathematics with Applications*, 62(11), 4170–4177.

Liu, Y., Ding, F., and Shi, Y. (2012). Least squares estimation for a class of non-uniformly sampled systems based on the hierarchical identification principle. *Circuits, Systems, and Signal Processing*, 31(6), 1985–2000.

Liu, Y. and Bai, E.W. (2007). Iterative identification of hammerstein systems. *Automatica*, 43(2), 346–354.

Oh, S.Y. and Park, D.J. (2000). Design of novel two-layered fuzzy logic controller for plants with time-varying dead-zone and saturation characteristics. *Journal of Intelligent & Fuzzy Systems,* 8(3), 173–190.

Pan, J., Li, W., and Zhang, H. (2018). Control algorithms of magnetic suspension systems based on the improved double exponential reaching law of sliding mode control. *International Journal of Control, Automation and Systems*, 16(6), 2878–2887.

Pu, Y., Yang, Y., and Chen, J. (2021). Some stochastic gradient algorithms for hammerstein systems with piece- wise linearity. *Circuits, Systems, and Signal Processing*, 40(4), 1635–1651.

Schoukens, M. and Tiels, K. (2017). Identification of block-oriented nonlinear systems starting from linear approximations: A survey. *Automatica*, 85, 272–292.

Tahoun, A. (2017). A new online delay estimation-based robust adaptive stabilizer for multi-input neutral systems with unknown actuator nonlinearities. *ISA transactions*, 70, 139–148.

Xia, G., Shao, X., Zhao, A., and Wu, H. (2013). Adaptive neural network control with backstepping for surface ships with input dead-zone. *Mathematical Problems in Engineering*, 2013.

Xie, L. and Yang, H. (2017). Auxiliary model based multi-innovation stochastic gradient identification algorithm for periodically non-uniformly sampled-data hammerstein systems. *algorithms*, 10(3), 84.

Xie, L., Yang, H., and Ding, F. (2017). Identification of non-uniformly sampled-data systems with asynchronous input and output data. *Journal of the Franklin Institute*, 354(4), 1974–1991.

Xie, L., Yang, H., Ding, F., and Huang, B. (2016). Novel model of non-uniformly sampled-data systems based on a time-varying backward shift operator. *Journal of Process Control*, 43, 38–52.

Xing, L., Wen, C., Su, H., Cai, J., and Wang, L. (2015). A new adaptive control scheme for uncertain nonlinear systems with quantized input signal. *Journal of the Franklin Institute*, 352(12), 5599–5610.

Xu, L. (2017). The parameter estimation algorithms based on the dynamical response measurement data. *Advances in Mechanical Engineering*, 9(11), 1687814017730003.

Xu, L., Xiong, W., Alsaedi, A., and Hayat, T. (2018). Hierarchical parameter estimation for the frequency response based on the dynamical window data. *International Journal of Control, Automation and Systems*, 16(4), 1756–1764.

Zhang, J., Yu, F., and Chin, K. (2017). Recursive identification of hammerstein systems with dead-zone nonlinearity in the presence of bounded noise. *International Journal of Systems Science*, 48(11), 2394–2404.

Zhou, L., Li, X., Shan, L., Xia, J., and Chen, W. (2017). Hierarchical recursive least squares parameter estimation of non-uniformly sampled hammerstein nonlinear systems based on kalman filter. *Journal of the Franklin Institute*, 354(10), 4231–4246.